# Graphene Contact Engineering in VP/$MoS_2$ Van der Waals Heterostructures for High Performance, Durable and Multispectral Photodetection

Waqas Ahmad[a, ǁ,*], Umer Younis[b, ǁ], Muhammad Zubair Nawaz[a], Jinying Zhang[c], Wen Lei[d], Qiandong Zhuang[e,*], Zhiming Wang[f,g,*], Yury Illarionov [a,*]

[a]Laboratory of 2D Optoelectronics and Nanoelectronics (L2DON), Department of Materials Science and Engineering, Southern University of Science and Technology, 1088 Xueyuan Blvd, Shenzhen, 518055 China

[b]Department of Chemistry, Southern University of Science and Technology, 1088 Xueyuan Blvd, Shenzhen, 518055 China

[c]State Key Laboratory of Electrical Insulation and Power Equipment, Center of Nanomaterials for Renewable Energy, School of Electrical Engineering, Xi'an Jiaotong University, Xi'an, Shaanxi 710049, China

[d]Department of Electrical, Electronic and Computer Engineering, The University of Western Australia, Crawley, WA, 6009 Australia

[e]Physics Department, Lancaster University, Lancaster, LA14YB UK

[f]School of Physics, University of Electronic Science and Technology of China, Chengdu 610054 China

[g]Shimmer Center, Tianfu Jiangxi Laboratory, Chengdu 641419, China

**Corresponding authors**

W. Ahmad, waqas@sustech.edu.cn

Q. Zhuang, q.zhuang@lancaster.ac.uk

Z. Wang, zhmwang@uestc.edu.cn

Y. Illarionov, illarionov@sustech.edu.cn

‖ Waqas Ahmad and Umer Younis are equally contributed to this work.

**Table of Contents**

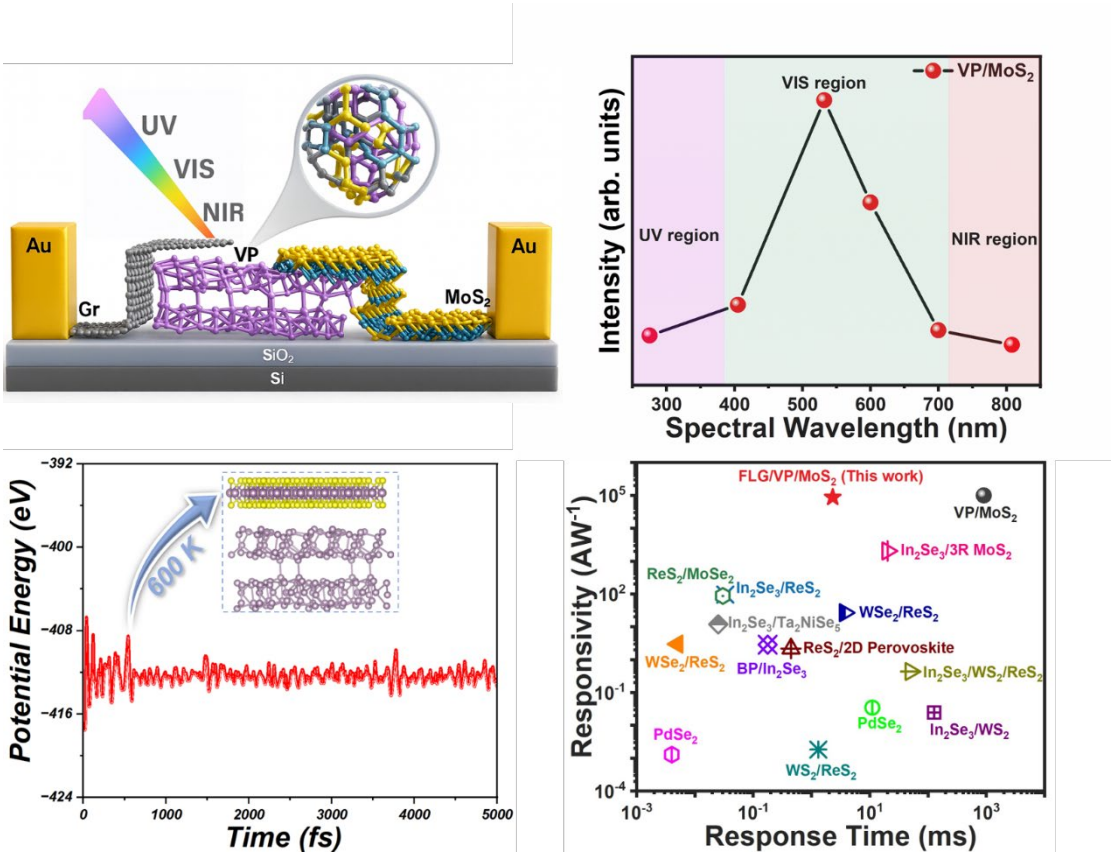

**Abstract**

Efficient photocarrier separation and collection are essential for high-performance photodetectors. In van der Waals (vdWs) heterostructures, carefully engineering on the interfaces and built-in electric fields is an effective strategy to maximize device performance. Here, we present a unique photodetector based on a vertically stacked few-layer graphene/violet phosphorus/$MoS_2$ (FLG/VP/$MoS_2$) vdWs heterostructure, which exhibits significantly enhanced performance across a broad spectral range from ultraviolet (275 nm) to near Infrared (808 nm). The photodetector achieves a responsivity of up to $8.8\times10^4$ A/W with an external quantum efficiency of $1.81\times10^7$ values over five orders of magnitude higher than of bare VP/$MoS_2$ device (~0.52 A/W, 7.68%, respectively). It also exhibits a fast photoresponse (rise time ~2.3 ms) and notable polarization sensitivity (dichroic ratio ~1.075). Moreover, the device maintains stable performance over at least 100 on-off cycles, highlighting its excellent operational durability. First-principles (DFT) calculations further corroborate the strong interlayer coupling and structural stability of the device interface, providing theoretical support for the observed durability and photodetection mechanism. Collectively, this work positions the FLG/VP/$MoS_2$ vdWs heterostructure as a promising platform for high-performance, broadband, and polarization-sensitive photodetection in advanced optoelectronic applications.

**Keywords:** Graphene contact engineering; 2D materials; Violet phosphorus; Heterostructures; Photodetectors; Responsivity

## 1. Introduction

Photodetectors are central to modern optical sensing and communications; however, many traditional designs struggle to deliver the required sensitivity and speed across broad wavelength ranges [1, 2]. Conventional photodetectors which are exemplified by silicon-based devices are suffers from limited responsivity (R), slow response times, and a narrow range of detectable wavelengths [3]. These inherent limitations impede their use in advanced applications that demand simultaneous ultraviolet (UV) to near infrared (NIR) detection and rapid signal processing [4]. As a result, there is a strong impetus to develop new photodetector architectures that overcome these shortcomings, achieving higher sensitivity over multi-spectral bands while maintaining fast response and long-term stability [5].

One promising approach is to leverage emerging nanoscale materials, particularly two-dimensional (2D) materials and their van der Waals (vdWs) heterostructures which are important to engineer photodetectors with superior performance [6, 7]. Atomically thin 2D semiconductors such as graphene and transition metal dichalcogenides (TMDCs) such as $MoS_2$, $WS_2$, $MoSe_2$, $WSe_2$ etc. exhibit exceptional photoelectronic properties, including high carrier mobilities and tunable bandgaps, which can be tailored to enhance photodetection efficiency [7, 8]. By vertically stacking 2D materials without the constraints of lattice matching, vdWs heterostructures enable the combination of multiple functional materials in a single device, therefore which can enhance the photodetection sensitivity and also realize broaden photoresponse across multiple spectrums [9, 10]. For example, a group of researchers explored violet phosphorus

(VP)/$MoS_2$ vdWs heterostructure device shows high R of $10^5$ A/W, detectivity (D*) of $10^{13}$ Jones and an external quantum efficiency (EQE) of $10^7$% at the wavelength of 532 nm. They noticed that, their VP/$MoS_2$ vdWs heterostructure device's performance are better than their individual VP and $MoS_2$ photodetector device [11]. Another, a group of researchers demonstrated vdWs heterostructure device based on the VP/InSe which is showing broadband spectrum response from visible (VIS) to NIR including a high R of 182.8 A/W, an excellent D* of $10^{12}$ Jones and an EQE of 11939% [12]. Recently, a combination of 2D materials such as $TaSe_2/WS_2/TaSe_2$ in the form of vdWs heterostructure enables excellent photoelectronic characteristics such as a high R of 292 mA/W, an outstanding D* of $10^{11}$ Jones and large optical switching ratio of $10^5$ at the wavelength of 633 nm. In addition, demonstrated device shows excellent stability over 3 months [13]. Such examples underscore how 2D materials stacks can deliver detection capabilities far beyond those of any single bulk semiconductor, offering a clear pathway toward high-performance, multispectral photodetection [14, 15].

Among the family of 2D materials, VP, a lesser-known layered allotrope of phosphorus, has recently emerged as a highly promising alternative [16]. As the most stable phosphorus allotrope, VP exhibits significantly improved resistance to oxidation and degradation compared to black phosphorus (BP) [17]. At the same time, it retains the desirable anisotropic optical response of phosphorene [18]. VP has a unique tubular crystal structure that gives rise to strongly direction-dependent (polarization-sensitive) light matter interactions and a relatively large bandgap [19]. For example, bulk and few-layer of VP feature a direct bandgap of 1.8-2.5 eV (reaching ~2.5 eV in the monolayer

limit) and can support high hole mobilities up to 7000 $cm^2V^{-1}s^{-1}$ [20]. These properties indicate that VP can serve as an excellent 2D semiconductor for photodetectors, offering broad spectral absorption in the broadband spectrum range, polarization sensitivity, and robust air stability. On the other hand, $MoS_2$ is a well-explored 2D material that belongs to the TMDCs family and is widely used for optoelectronic devices [21-23]. Integrating VP and $MoS_2$ in a single device as a vertically vdWs structure can be expected to deliver not only broadband photodetection but also reliable performance under ambient conditions. Such a synergistic combination paves the way for developing next-generation photodetectors with enhanced efficiency and stability. Furthermore, device performance can be optimized by contact engineering, for instance by using a graphene electrode. Such contact engineering can reduce contact resistance and energy barriers at the interface, thereby facilitating more efficient charge injection and collection. For example, $InSe/WSe_2$ with graphene electrodes can enhance photodetection performance including a high R of 829.7 A/W, an excellent D* of upto $10^{14}$ Jones and rapid photoresponse of 10 μs [24]. In addition, another group of researchers demonstrated $Gr/InSe/MoTe_2$ vdWs heterostructure device which can enable to reduce dark current upto $10^{-14}$ A and quick photoresponse of 14 μs. These results attributed to the narrow bandgap of the graphene as compared to gold (Au), resulting in a nearly negligible Schottky barrier at the graphene-InSe interface [25]. Such an optimized interface enables enhanced photodetection performance by reducing recombination losses and boosting carrier transport. Building on this concept, the device architecture can be further extended to achieve broadband response and

multifunctional applications in advanced optoelectronic systems.

In this work, we present a photodetector based on a vertically stacked FLG/VP/$MoS_2$ vdWs heterostructure, designed to significantly enhance photodetection performance. In this device geometry, FLG was incorporated on the VP side, which not only improves the stability of VP but also reduces the interface barrier between VP and Au contacts. As a result of this engineering strategy, the device demonstrates an excellent broadband photodetection response from the 275 nm to 808 nm, achieving a high R of $8.8\times10^4$ A/W and an outstanding EQE of $1.81\times10^7$%, which are more than five orders of magnitude higher than the bare VP/$MoS_2$ photodetector (0.52 A/W and 7.68%). In addition, the FLG/VP/$MoS_2$ photodetector exhibits a rapid photoresponse of ~2.3 ms along with a measurable polarization sensitivity of 1.075, underscoring its strong potential for multifunctional use in advanced photodetection and polarization-sensitive optoelectronic systems. Furthermore, DFT calculations confirm robust interlayer coupling and structural stability at the FLG/VP/$MoS_2$ interface, and molecular dynamics simulations at 600 K further verify its thermal durability. Moreover, the calculated bandgap of the VP/$MoS_2$ heterostructure is ~1 eV, indicating intrinsic sensitivity in the near-infrared region, which is consistent with our experimental findings. Overall, this research provides a promising pathway toward the development of next-generation high-performance photodetectors.

## 2. Experimental section

### *2.1 Device fabrication*

Few-layer VP and $MoS_2$ flakes were obtained through mechanical exfoliation from

high-purity bulk crystals (~99.999%, 2D Semiconductors). For device fabrication of VP/$MoS_2$, VP flakes were first exfoliated onto pre-cleaned p-type $SiO_2$/Si substrates using the conventional scotch tape method. Prior to exfoliation, the $SiO_2$/Si substrates were cleaned by sequential sonication in acetone and isopropyl alcohol for 15 minutes each, and then dried with a gentle nitrogen stream. Subsequently, few-layer $MoS_2$ flakes were exfoliated onto a PDMS stamp and precisely transferred onto the VP flakes using a dry-transfer method, forming the VP/$MoS_2$ vdWs heterostructure. Graphene flakes were also prepared via the scotch tape method and transferred onto the VP side with the assistance of a PDMS stamp, completing the Gr/VP/$MoS_2$ heterostructure. Finally, maskless photolithography (TuoTuo Technologies, Suzhou Co., Ltd.) was applied to define the electrode regions, and Au (50 nm) contacts were deposited by thermal evaporation to finalize the device assembly.

*2.2. characterization*

The thickness of the Gr/VP/$MoS_2$ vdWs heterostructure was determined using an Atomic Force Microscope (Bruker Dimension Icon, Germany). Surface potential mapping was carried out on the same instrument operating in scanning probe mode. Raman and PL spectroscopy was performed with a Horiba LabRAM HR Evolution system (Japan) using a 532 nm excitation laser. Photoelectrical characterizations, including broadband photodetection, were conducted using a wavelength-tunable monochromatic light source (https://bjnbet.com/) coupled with a Keithley 2638B source meter. Polarization-resolved photocurrent measurements were performed on a customized setup from TuoTuo Technologies (Suzhou, China), integrated with a

Keithley 2612B source meter. The optical power of the incident light was continuously monitored with a Thorlabs PM101 power meter. All fabrication and measurement processes were carried out under ambient conditions at room temperature.

## 3. Results and discussion

### *3.1. Device fabrication and characterization*

The schematic of the FLG/VP/$MoS_2$ vdWs heterostructure device is shown in **Fig. 1**a, with a magnified view of the material interfaces. **Fig. 1**b exhibits the optical image of the FLG/VP/$MoS_2$ vdWs heterostructure device. In this device structure, FLG, VP and $MoS_2$ obtained by mechanical exfoliation (details in experimental section). Atomic force microscopy (AFM) was used to examine the device surface morphology (**Fig. 1**c). Thickness profiles taken along the red (VP), green ($MoS_2$) and blue (FLG) lines yield layer thicknesses of approximately 8 nm (VP), 8 nm ($MoS_2$), and 7 nm (FLG) as summarized in Figure **S1a-c** (**Supporting Information**). These measurements confirm the successful assembly of the vdWs heterostructure device of FLG/VP/$MoS_2$. Raman measurements were performed to assess material quality for the heterostructure device of VP/$MoS_2$. The Raman peaks for VP observed at 353, 373, and 471 $cm^{-1}$, which are attributed to the $A_g$ and $B_g$ modes as depicted in Figure **S2a** (**Supporting Information**). For the $MoS_2$ nanoflakes, the Raman spectra observed at 383 and 408 $cm^{-1}$ correspond to the $E_{2g}^1$ and $A_{1g}$ vibrational modes as illustrated in Figure **S2b** (**Supporting Information**). Raman spectra of VP/$MoS_2$ are well consistent with previous reports [11, 26]. The coexistence of these Raman features in the overlapping region confirms the successful formation of the VP/$MoS_2$ heterostructure as shown in Figure **S2c**

(**Supporting Information)**. To further explore the interfacial optoelectronic properties, photoluminescence (PL) measurements were carried out. As shown in **Fig. 1**d, the PL intensity of $MoS_2$ is significantly quenched in the heterostructure compared to that of bare $MoS_2$. This quenching effect evidences efficient charge transfer and electron-hole separation at the interface, which plays a crucial role in enhancing the performance of photodetectors.

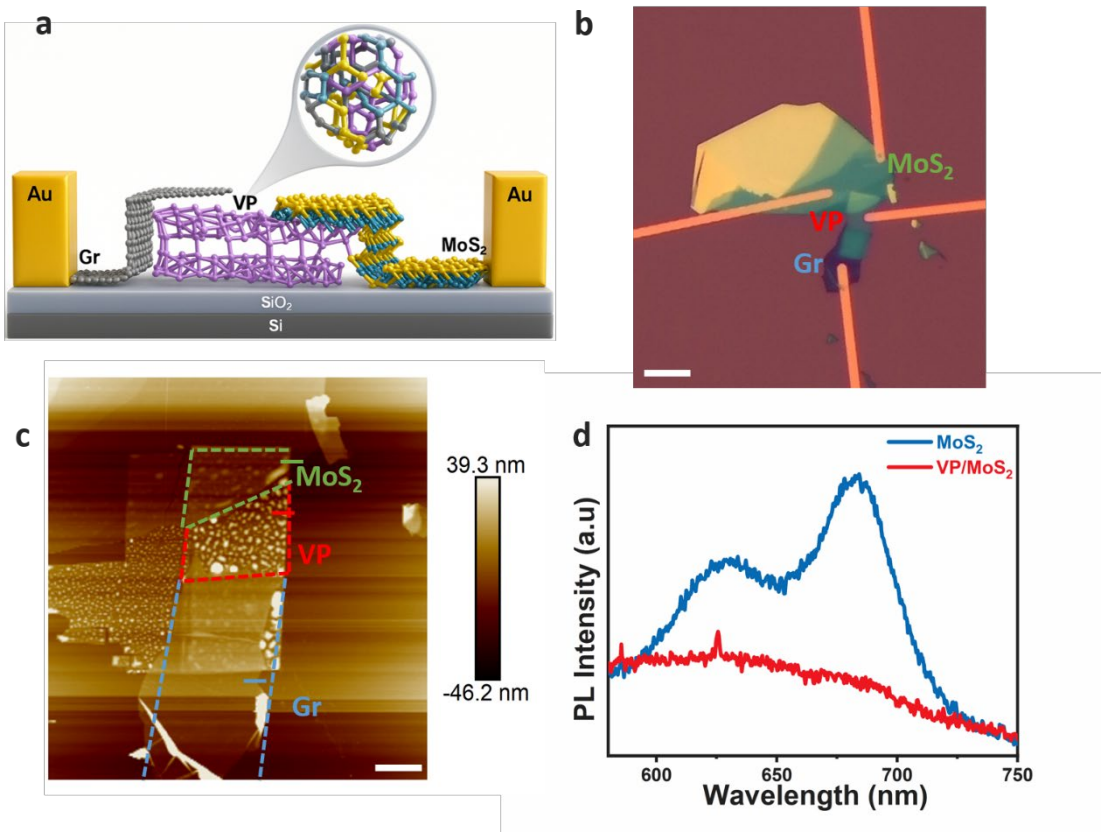


**Fig. 1.** Device fabrication and characterization. (a, b) Schematic illustration of FLG/VP/$MoS_2$ based vdWs heterostructure and optical image of the corresponding device, scale bar = 10 µm. (c) AFM image of the device of FLG/VP/$MoS_2$ based vdWs heterostructure. PL spectra of MoS2 and VP/$MoS_2$ vdWs heterostructure.

*3.2 Photodetection characteristics*

Before evaluating the photodetection characteristics of the FLG/VP/$MoS_2$ photodetector device, we first characterized the photoresponse of the bare VP/$MoS_2$ photodetector device. As shown in **Fig. 2**a, the VP/$MoS_2$ device exhibits a broadband spectral response from 275 nm to 808 nm, with a pronounced peak at 532 nm. Notably, clear photoresponse signals are observed at the UV (275 nm) and NIR (808 nm) edges Figure **S3a-d** (**Supporting Information**). However, this bare VP/$MoS_2$ device produces only a very low photocurrent on the order of $10^{-11}$ A. To improve the photocurrent, we integrated FLG on the VP side of the heterostructure to reduce the Schottky barrier and contact resistance, thereby enhancing the device performance [27]. For the FLG/ VP/$MoS_2$ photodetector device, the output characteristics (**Fig. 2**b) reveal a pronounced photoconductive effect in this vdWs heterostructure of FLG/ VP/$MoS_2$. This indicates that an external bias is required to operate the device, and it confirms that the device functions as a photodetector under 532 nm illumination. The FLG/VP/$MoS_2$ photodetector device can even operate under a very low incident power density of 0.19 mW/$cm^2$, demonstrating its high sensitivity (**Fig. 2**c). Furthermore, the FLG/ VP/$MoS_2$ device retains a broadband spectral response similar to the bare device (Fig. **S4a,b Supporting Information**). **Fig. 2**d demonstrates the device's time-resolved photoresponse under chopped 532 nm laser illumination at various power levels, showing stable on/off switching behavior. When the light is turned on, the photocurrent rises rapidly to a steady value. Once the light is switched off, it quickly returns to the baseline, reflecting the device's high sensitivity and reversibility. Similarly, the bare

VP/$MoS_2$ photodetector device exhibits the same stable on/off photocurrent behavior (Fig. **S5a,b Supporting Information**). In addition, we evaluated the photodetector's performance using key figures of merit, specifically R and EQE. The R is defined as:

$$R = I_{ph}/(P_{in}A) \quad (1)$$

where $I_{ph}$ denoted the photocurrent, calculated as the difference between the illuminated current ($I_{light}$-$I_{dark}$). $P_{in}$ expresses as the incident light power density, while A corresponds to the effective active area of the photodetector.

$$\mathrm{EQE} = \frac{\mathrm{Iph/q}}{\mathrm{Pin/hv}} \quad (2)$$

In the above relation, where h denotes Planck's constant, q is the elementary charge, and v represents the frequency corresponding to the wavelength of the incident light. Using these relations, the FLG/VP/$MoS_2$ photodetector device achieved a maximum R $8.8\times10^4$ A/W and $1.81\times10^7$%, which are more than five orders of magnitude higher than those of the VP/$MoS_2$ photodetector device ($5.2\times10^{-1}$ A/W and 7.68%, respectively) as shown in **Fig. 2**e,f. This exceptional improvement is attributed to the reduced Schottky barrier and greatly enhanced interfacial charge transfer afforded by the graphene contact.

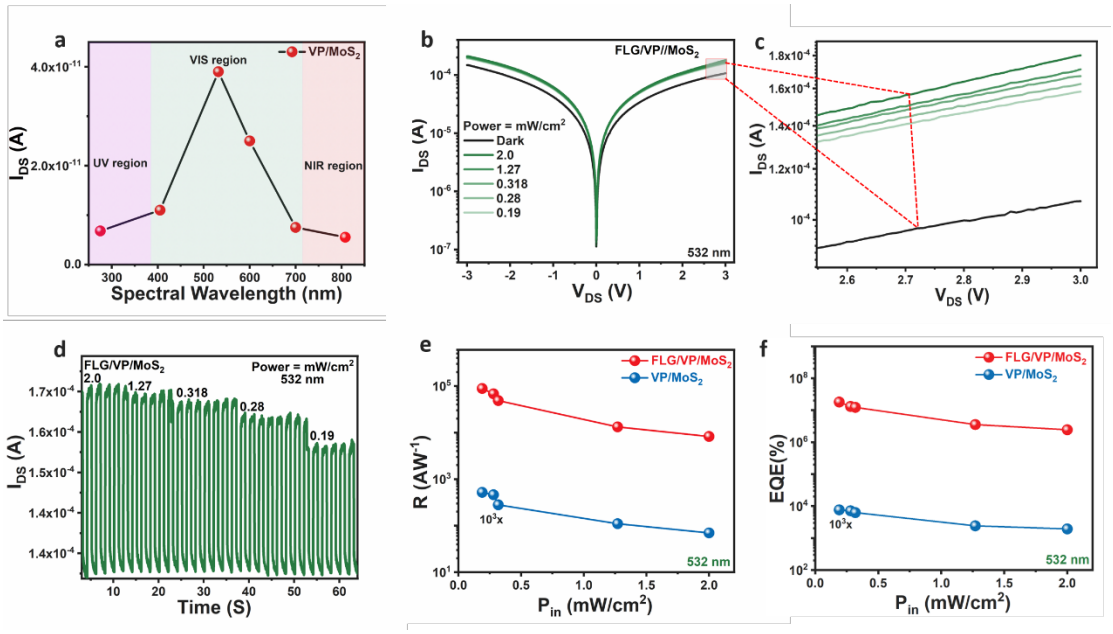


**Fig. 2.** Photodetection characterizations of FLG/VP/$MoS_2$ photodetector device. (a) Spectral photoresponse of the VP/$MoS_2$ photodetector device measured across 275 nm - 808 nm. (b) Typical output characteristics of the VP/$MoS_2$ photodetector device under dark and different illuminated conditions at the wavelength of 532 nm. (c) Enlarged view of the photocurrent evolution with increasing optical power density. (d) Time-resolved photoresponse of the VP/$MoS_2$ photodetector device under different optical power density at the wavelength of 532 nm. (e) Responsivity of VP/$MoS_2$ and Gr/VP/$MoS_2$ photodetector devices as a function of different incident optical power density. (f) External quantum efficiency comparison of VP/$MoS_2$ and Gr/VP/$MoS_2$ photodetector devices at 532 nm under different optical excitation power densities.

The photoresponse speed is a critical metric for evaluating photodetector performance. It is commonly quantified by the rise time and fall time, defined as the intervals for photocurrent to increase from 10% to 90% of its peak value and decay from 90% down

to 10%, respectively. In our devices, both the VP/$MoS_2$ vdWs heterostructure and the FLG/VP/$MoS_2$ vdWs heterostructure exhibit ultrafast response speeds. Specifically, the VP/$MoS_2$ photodetector device shows a rise time of ~5.1 ms and fall time of ~8.7 ms, while the FLG/VP/$MoS_2$ photodetector device achieves an even faster rise/fall time of ~2.3 ms/~7.5 ms (**Fig. 3**a,b). The significantly faster response of the FLG/VP/$MoS_2$ photodetector device is attributed to the integration of the FLG as an contact engineering, which improves charge transport and extraction. Graphene forms a clean, conductive contact that reduces interfacial trap states and lowers the Schottky barrier, allowing photogenerated carriers to be collected more rapidly. In essence, graphene's high mobility and Fermi-level alignment help sweep out photo-excited carriers quickly, minimizing charge trapping and recombination at the interfaces. This leads to a markedly quicker on/off switching of photocurrent in the FLG/VP/$MoS_2$ photodetector device compared to the VP/$MoS_2$ photodetector device alone. We further investigated the power-dependent photocurrent characteristics of both devices (Fig. **S6a,b Supporting Information**). The relationship between photocurrent ($I_{ph}$) and incident optical power ($P_{in}$) can be expressed as $I_{ph} \propto P_{in}^{\alpha}$ where the exponent $\alpha$ ($0 < \alpha \leq 1$) provides insight into carrier dynamics under varying illumination intensities. An ideal linear photodetector would have $\alpha \approx 1$ (meaning photocurrent scales linearly with light power), whereas $\alpha < 1$ indicates sublinear behaviour often caused by effects like carrier recombination, trap-assisted photogating, or saturation of trap states at higher illumination. For our VP/$MoS_2$ photodetector device, we obtained a fitted $\alpha \approx 0.70$ at 532 nm, indicating a moderately sublinear response. In contrast, the FLG/VP/$MoS_2$

device shows a much lower exponent, $\alpha \approx 0.13$ at 532 nm, revealing a strongly sublinear dependence on power.

To explore polarization sensitivity, we measured the photocurrent of the FLG/VP/$MoS_2$ photodetector device as a function of incident light polarization angle. (Fig. **S7, Supporting Information**) shows the schematic of our polarization-dependent photodetection setup. The polarization angle θ is defined as the angle between the incident light's polarization direction and the crystallographic a-axis of the photodetector [28]. Using a half-wave plate, θ was varied continuously from 0° to 360°, and we recorded the photocurrent at 15° increments to ensure comprehensive and reliable measurements. FLG/VP/$MoS_2$ photodetector device demonstrates clear angle-dependent photoresponse under 532 nm illumination (**Fig. 3**c), at a fixed incident power density of 2.0 mW/cm$^{-2}$. The measured polarization-dependent photocurrent follows a sinusoidal pattern accurately described by the equation below [29]:

$$I_{ph}(\alpha) = I_a cos^2(\alpha + \beta) + I_b cos^2(\alpha + \beta) sin^2(\alpha + \beta) + I_c sin^2(\alpha + \beta) \quad (3)$$

In the above relation, $I_a$, $I_b$ and $I_c$ are related to the photocurrent, while α represents the polarization angle and β is a constant offset angle. **Fig. 3**d shows polar plots that further emphasize the polarization nature of photodetection at each angle. FLG/VP/$MoS_2$ photodetector device, we extracted a dichroic ratio of ~1.076, meaning the photocurrent in the preferred polarization is about 7.6% higher than in the orthogonal polarization. This dichroic ratio is somewhat lower than those reported for photodetectors made from other highly anisotropic 2D materials or their heterostructures (in many cases, dichroic ratios of 2-3 or higher have been achieved with materials like black phosphorus, $ReS_2$,

etc.) [30-32]. The comparatively low polarization contrast in our device can be explained by the influence of $MoS_2$ and graphene. In the FLG/VP/$MoS_2$ photodetector device, the isotropic $MoS_2$ layer dilutes the anisotropic response of the VP. Essentially, some fraction of the photocurrent is generated or conducted through $MoS_2$ (and graphene contacts) in a polarization-insensitive manner, thereby reducing the overall contrast between different polarization angles. Additionally, the stacking and coupling of layers may slightly reduce the anisotropy of VP's absorption (for instance, if the VP's absorption peak is not extremely strong at 532 nm or if multi-layer VP is used, the intrinsic anisotropy might not be as pronounced). As a result, the device shows only a mild polarization dependence (dichroic ratio ~1.076), which is lower than devices using purely anisotropic crystals, but still demonstrates the ability to discern polarization to a degree. Despite the modest dichroic ratio, our FLG/VP/$MoS_2$ photodetector device achieves a well-balanced performance when compared with other state-of-the-art 2D material and their vdWs heterostructures photodetector devices at VIS spectrum **(Fig. 3**e,f) [33-50]. Notably, the FLG/VP/$MoS_2$ photodetector device simultaneously delivers high R, fast response speed and moderate dichroic ratio.

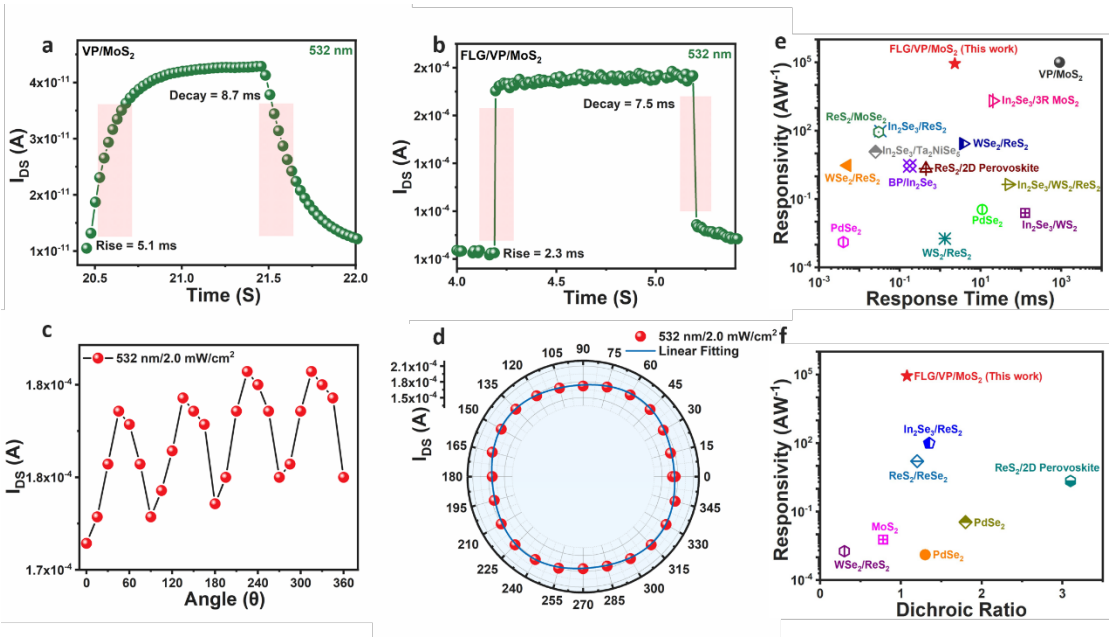


**Fig. 3.** Photoresponse and polarization characterization. (a, b) Time resolved photoresponse of the VP/$MoS_2$ and FLG/VP/$MoS_2$ photodetector devices at the wavelength of 532 nm, respectively, $V_{ds}$ = 1V, Pin = 2.0 mW/$cm^2$. (c, d) Photoresponse as a function of polarization angle (0°-360°) at wavelength of the 532 nm for the FLG/VP/$MoS_2$ photodetector device, respectively, $V_{ds}$ = 1V, Pin = 2.0 mW/$cm^2$. (e, f) Performance comparison of R Vs. Response time and R Vs. Dichroic ratio FLG/VP/$MoS_2$ photodetector device with others 2D materials and their vdWs photodetectors technologies.

*3.3 Durability and stability*

To assess the theoretical durability of the FLG/VP/$MoS_2$ vdWs heterostructure, DFT calculation performed at 600 K for a 5 ps trajectory. The potential energy remained nearly constant throughout the simulation (**Fig. 4**a), fluctuating only minimally around an equilibrium value. This stable energy profile indicates excellent thermal stability of the heterostructure at elevated temperature, with no signs of structural degradation or

bond breaking over the simulation timeframe. Such robust atomic-scale stability suggests that the layered FLG/VP/$MoS_2$ system can withstand significant thermal stress, providing a strong foundation for reliable device operation. Importantly, the experimental results corroborate this theoretical prediction of stability. **Fig. 4**b,d present the time-resolved photoresponse of VP/$MoS_2$ and FLG/VP/$MoS_2$ photodetector devices, respectively, under 532 nm illumination ($V_{ds}$ = 1 V) over 100 on-off cycles. In both devices, the photocurrent response remains strong and repeatable from the first cycle to the hundredth, with no appreciable decay in intensity or alteration of response speed. **Fig. 4**c,e zoom into the last five switching cycles of each device, highlighting that the photogenerated signal amplitude and timing are consistent even at the end of the 100-cycle test. Notably, no encapsulation was used in these measurements, the devices were exposed to ambient conditions yet they maintained robust performance throughout. This enduring stability under repetitive optical cycling can be attributed to the intrinsic resilience of the VP/$MoS_2$ vdWs heterostructure. In particular, integrating a FLG capping layer (FLG/VP/$MoS_2$) appears to further preserve device integrity by passivating the VP and providing an efficient charge transport pathway. The excellent agreement between the DFT calculations (predicting a thermally stable structure) and the sustained experimental photoresponse confirms that the VP/$MoS_2$ and FLG/VP/$MoS_2$ vdWs heterostructures are highly durable.

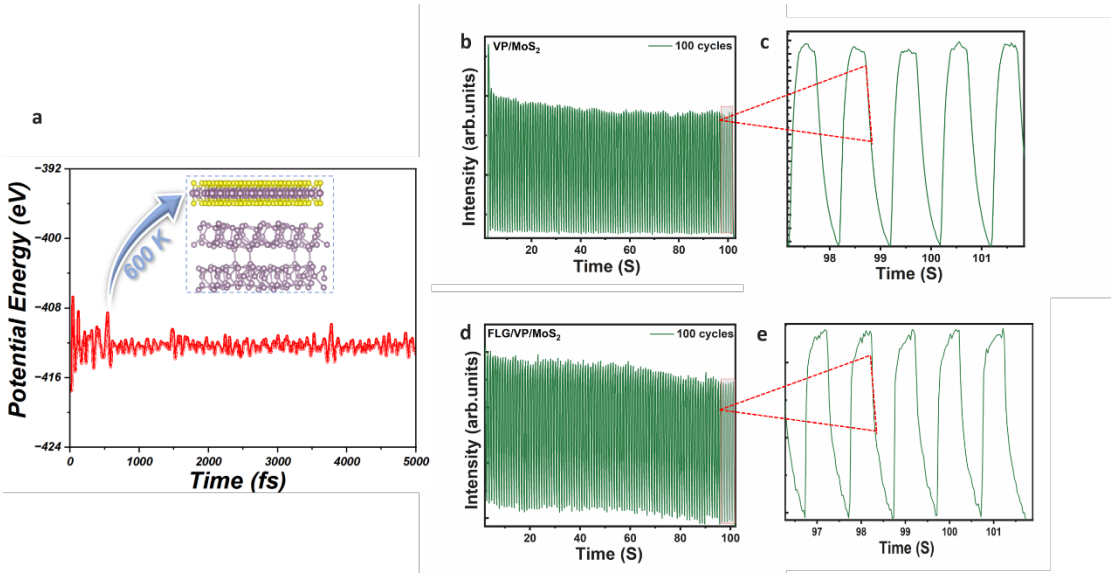


**Fig. 4.** Durability and stability. (a) Theoretical calculations of VP/$MoS_2$ vdWs heterostructure at 600 K for 5 ps, showing a stable potential energy trace over time and indicating excellent thermal stability of the structure. (b, d) Time-resolved photoresponse of the VP/$MoS_2$ and FLG/VP/$MoS_2$ photodetector device under 532 nm light ($V_{ds}$ = 1 V) respectively for 100 on-off cycles, demonstrating stable and repeatable photocurrent with no significant degradation over the cycling period. (c, e) Enlarged view of the last five cycles from (b, d), highlighting consistent signal amplitude and switching behavior up to the 100th cycle.

*3.4 Photodetection mechanism*

We then systematically investigated the photodetection mechanism between the FLG, VP and $MoS_2$. The VP/$MoS_2$ vdWs heterostructure (**Fig. 5**a) was first analyzed via DFT. The hybrid HSE06 functional yields an electronic band structure for the VP/$MoS_2$ bilayer with a predicted bandgap of approximately 1.0 eV (**Fig. 5**b). This moderate gap lies in the NIR range, indicating that the coupled material system can absorb and respond to long wavelengths. Indeed, a 1 eV gap corresponds to a photon wavelength

of ~1240 nm, so the heterostructure device of VP/$MoS_2$ is expected to be sensitive well into the NIR which is consistent with our experimental observation of photodetection up to 808 nm (**Fig. 2**a). The DFT band structure also suggests a type-II band alignment. The valence band maximum (VBM) and conduction band minimum (CBM) reside predominantly on different layers (VP and $MoS_2$, respectively).

To further elucidate the electronic contribution of individual atoms, the projected density of states (PDOS) was calculated (Fig. **S8, Supporting Information**). The PDOS shows that the states VBM are dominated by P orbitals, whereas the conduction CBM primarily originates from Mo d-orbitals with partial contributions from S. This orbital-resolved picture corroborates the type-II alignment deduced from the band structure. For example, holes preferentially localize in VP while electrons are stabilized in $MoS_2$. Such orbital distribution not only confirms the staggered band alignment but also highlights the efficient charge-transfer pathway across the interface, which is essential for high-performance photodetection.

To validate the predicted band alignment and its role in photodetection, we employed Kelvin probe force microscopy (KPFM) to map the surface potential of the FLG /VP/$MoS_2$ vdWs heterostructure. As shown in **Fig. 5**c, a line scan along the white dashed path sequentially traverses Gr-VP-$MoS_2$, enabling extraction of local surface-potential variations across each interface (**Fig. 5**c). The contact potential difference (CPD) between the probe tip and the sample is mathematically expressed as follows:

$$V_{CPD} = (W_{tip} - W_{sample})/e \quad (4)$$

where represents the elementary charge, $W_{tip}$ denotes the work function of the KPFM

tip, and $W_{sample}$ corresponds to the work function of the sample. Using this relation, KPFM measurements reveal a contact potential difference ($V_{CPD}$) of approximately 264 mV at the VP/$MoS_2$ vdWs heterostructure interface (**Fig. 5**d). Based on the KPFM calculations, the energy band diagram of Gr/VP/$MoS_2$ vdWs heterostructure before contact and after contact were plotted as shown in **Fig. 5**e,f. respectively. According to the band alignment, upon illumination, electron-hole pairs generated in both VP and $MoS_2$ are separated by the built-in field at the VP-$MoS_2$ heterojunction. Electrons transfer from VP into the lower-lying $MoS_2$ conduction band and drift through the channel toward the Au contact, while holes remain in VP; a fraction becomes trapped at VP/$MoS_2$ or interfacial states. These trapped holes act as a local positive gate on $MoS_2$ increasing the electron density and amplifying the channel current. The combination of type-II bands offsets, cooperative interfacial fields at VP/$MoS_2$ and $MoS_2$/Au that assist carrier separation and extraction. The theoretical band structure analysis (**Fig. 5**b) and the KPFM/band-alignment measurements (**Fig. 5**c-f) thus converge on a consistent picture that the VP/$MoS_2$ vdW heterostructure forms a type-II heterojunction with an ~1 eV gap, whose internal electric field and strong interfacial trapping enable efficient separation of electron-hole pairs and allow the device to detect NIR spectrum.

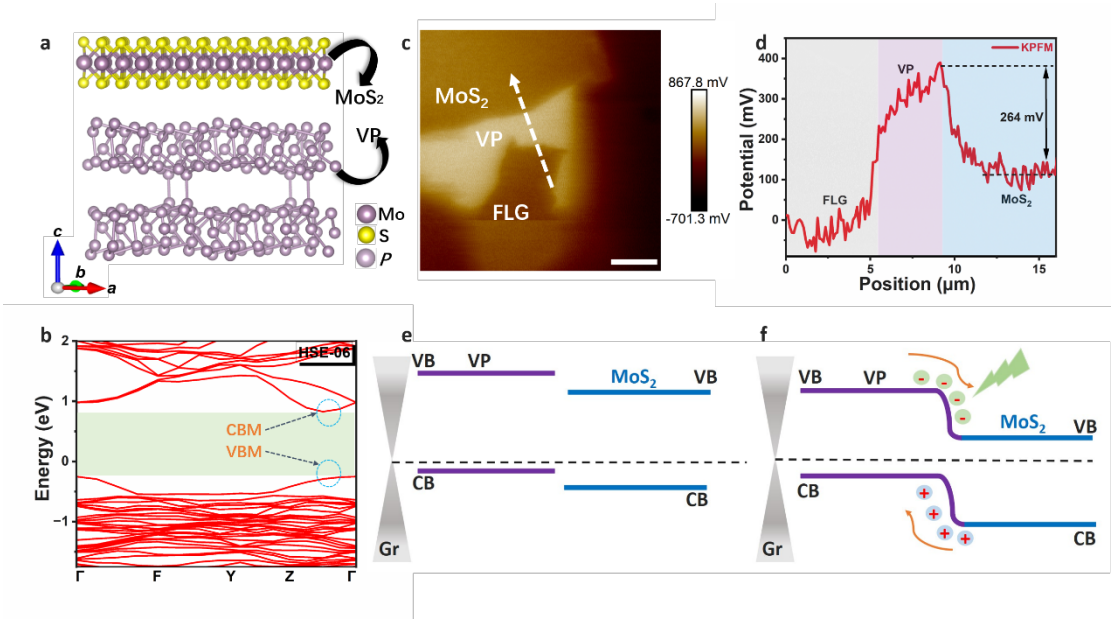


**Fig. 5.** Photodetection mechanism. (a) Atomistic structure of the vertically stacked VP/$MoS_2$ vdWs heterostructure (side view). Molybdenum (Mo) and sulfur (S) atoms of the $MoS_2$ layer and phosphorus (P) atoms of the VP layer are coloured to highlight the layered configuration. (b) Electronic band structure of the few-layer VP/$MoS_2$ bilayer calculated with the HSE06 hybrid functional. (c) KPFM surface potential map across the FLG/VP/$MoS_2$ vdWs heterostructure device, scale bar = 5 μm. (d) Line profile of the surface potential (contact potential difference, CPD) corresponding to the dashed arrow in (c), quantifying a ~264 mV potential step at the VP/$MoS_2$ junction. (e, f) Schematic energy band diagram of the FLG, VP, and $MoS_2$ before and after contact of illumination, illustrating the type-II band alignment.

## 4. Conclusions

In summary, a vertically stacked FLG/VP/$MoS_2$ vdWs heterostructure photodetector was fabricated, exhibiting a markedly enhanced broadband photoresponse. The device covers a spectral response range from 275 nm to 808 nm, with a high R of $8.8 \times 10^4$ A/W and an EQE of ~$1.81 \times 10^7$%, exceeding the bare device of VP/$MoS_2$ vdWs

heterostructure photodetector device by more than five orders of magnitude. It also shows a rapid photoresponse with a rise time of 2.3 ms, a good dichroic ratio of 1.075, and stable operation over at least 100 on-off cycles. The superior performance is attributed to the graphene layer, which stabilizes VP, enhances charge transport, and reduces interfacial barriers at the FLG/VP and VP/$MoS_2$ junctions. Furthermore, DFT calculations confirm strong interlayer coupling, structural stability and the thermal robustness of the VP/$MoS_2$ vdWs heterostructure. The calculated bandgap of ~1 eV for the VP/$MoS_2$ interface suggests intrinsic sensitivity in the NIR region, in excellent agreement with our experimental findings. Collectively, these results establish the FLG/VP/$MoS_2$ vdWs heterostructure device as a robust and durable platform for high-performance, broadband, and polarization-sensitive photodetection.

**Declaration of competing interest**

The authors declare that they have no known competing financial interests or personal relationships that could have appeared to influence the work reported in this paper.

**Data availability**

Data will be made available on request.

**Acknowledgments**

W.A and U.Y are equally contributed to this work. Y. I acknowledge the financial support from National Natural Science Foundation of China (NSFC) grant number W2432040, Guangdong Basic and Applied Basic Research Foundation 2023ZT10X010, 2024A1515010179, and Shenzhen Science and Technology Program 20231115150611001.

## Appendix A. Supplementary material

Supplementary data to this article can be found online at

## References


[1] M. Long, P. Wang, H. Fang, W. Hu, Progress, challenges, and opportunities for 2D material based photodetectors, Advanced Functional Materials 29(19) (2019) 1803807.

[2] F.P. García de Arquer, A. Armin, P. Meredith, E.H. Sargent, Solution-processed semiconductors for next-generation photodetectors, Nature Reviews Materials 2(3) (2017) 1-17.

[3] G. Konstantatos, Current status and technological prospect of photodetectors based on two-dimensional materials, Nature communications 9(1) (2018) 5266.

[4] C.-H. Liu, Y.-C. Chang, T.B. Norris, Z. Zhong, Graphene photodetectors with ultra-broadband and high responsivity at room temperature, Nature nanotechnology 9(4) (2014) 273-278.

[5] J. Liu, F. Xia, D. Xiao, F.J. Garcia de Abajo, D. Sun, Semimetals for high-performance photodetection, Nature materials 19(8) (2020) 830-837.

[6] K.S. Novoselov, A. Mishchenko, A. Carvalho, A. Castro Neto, 2D materials and van der Waals heterostructures, Science 353(6298) (2016) aac9439.

[7] M. Gibertini, M. Koperski, A.F. Morpurgo, K.S. Novoselov, Magnetic 2D materials and heterostructures, Nature nanotechnology 14(5) (2019) 408-419.

[8] W. Ahmad, J. Wu, Q. Zhuang, A. Neogi, Z. Wang, Research process on photodetectors based on group-10 transition metal dichalcogenides, Small 19(16) (2023) 2207641.

[9] W. Ahmad, M.Z. Nawaz, J. Kazmi, U. Younis, Y. Illarionov, Z. Wang, Two-Dimensional Indium Chalcogenides: From Fundamental Properties to Next - Generation Optoelectronic Devices, Advanced Optical Materials e01067.

[10] W. Ahmad, Y. Gong, G. Abbas, K. Khan, M. Khan, G. Ali, A. Shuja, A.K. Tareen, Q. Khan, D. Li, Evolution of low-dimensional material-based field-effect transistors, Nanoscale 13(10) (2021) 5162-5186.

[11] Y. Zhang, T. Zhu, N. Zhang, Y. Li, X. Li, M. Yan, Y. Tang, J. Zhang, M. Jiang, H. Xu, Air-Stable Violet Phosphorus/MoS2 van der Waals Heterostructure for High-Responsivity and Gate-Tunable Photodetection, Small 19(33) (2023) 2301463.

[12] W. Ahmad, M.U. Rehman, L. Pan, W. Li, J. Yi, D. Wu, X. Lin, H. Mu, S. Lin, J. Zhang, Ultrasensitive near-infrared polarization photodetectors with violet phosphorus/InSe van der Waals heterostructures, ACS Applied Materials & Interfaces 16(15) (2024) 19214-19224.

[13] X. Wang, L. Tong, W. Fan, W. Yan, C. Su, D. Wang, Q. Wang, H. Yan, S. Yin, Air-stable self-powered photodetector based on TaSe2/WS2/TaSe2 asymmetric heterojunction with surface self-passivation, Journal of Colloid and Interface Science 657 (2024) 529-537.

[14] W. Ahmad, L. Pan, K. Khan, L. Jia, Q. Zhuang, Z. Wang, Progress and insight of Van der Waals heterostructures containing interlayer transition for near Infrared photodetectors, Advanced Functional Materials 33(19) (2023) 2300686.

[15] W. Ahmad, J. Liu, J. Jiang, Q. Hao, D. Wu, Y. Ke, H. Gan, V. Laxmi, Z. Ouyang, F. Ouyang, Strong interlayer transition in few-layer InSe/PdSe2 van der Waals heterostructure for near-infrared

photodetection, Advanced Functional Materials 31(43) (2021) 2104143.
[16] W. Ahmad, A. Abbas, U. Younis, J. Zhang, S.H. Aleithan, Z. Wang, Advancements in optoelectronics: harnessing the potential of 2D violet phosphorus, Advanced Functional Materials 34(52) (2024) 2410723.
[17] A. Fali, M. Snure, Y. Abate, Violet phosphorus surface chemical degradation in comparison to black phosphorus, Applied Physics Letters 118(16) (2021).
[18] W. Chen, A. Chen, R. Zhang, J. Zeng, L. Zhang, M. Gu, C. Wang, M. Huang, Y. Guo, H. Duan, Strong in-plane optoelectronic anisotropy and polarization sensitivity in low-symmetry 2D violet phosphorus, Nano Letters 23(23) (2023) 10821-10831.
[19] L. Zhang, X. Li, F. Yao, L. Li, H. Huang, X. Zhao, S. Liu, Y. Cheng, H. Xu, J. Zhang, Fast identification of the crystallographic orientation of violet phosphorus nanoflakes with preferred in-plane cleavage edge orientation, Advanced Functional Materials 32(18) (2022) 2111057.
[20] A.G. Ricciardulli, Y. Wang, S. Yang, P. Samorì, Two-dimensional violet phosphorus: a p-type semiconductor for (opto) electronics, Journal of the American Chemical Society 144(8) (2022) 3660-3666.
[21] Y. Xie, B. Zhang, S. Wang, D. Wang, A. Wang, Z. Wang, H. Yu, H. Zhang, Y. Chen, M. Zhao, Ultrabroadband MoS2 photodetector with spectral response from 445 to 2717 nm, Advanced Materials 29(17) (2017) 1605972.
[22] A. Mirsepah, L. Shooshtari, R. Mohammadpour, A. Esfandiar, A. Irajizad, Wearable broadband MoS2 photodetector for dual heart rate and UV detection powered by PDMS-MXene TENG, Chemical Engineering Journal 499 (2024) 155953.
[23] X. Liu, J. Zhu, Y. Shan, C. Liu, C. Pan, T. Zhang, C. Liu, T. Chen, J. Ling, J. Duan, An ultrasensitive and broad - spectrum MoS2 photodetector with extrinsic response using surrounding homojunction, Advanced Science 11(45) (2024) 2408299.
[24] S.H. Aleithan, U. Younis, Z. Alhashem, W. Ahmad, Graphene electrode-enhanced InSe/WSe2 van der Waals heterostructure for high-performance broadband photodetector with imaging capabilities, Journal of Alloys and Compounds 1006 (2024) 176356.
[25] S. He, Y. Huang, C. Yin, Y. Ma, A. Shan, T.R. Wei, M. Li, L. Zhao, L. Gao, Self-powered and vis-infrared broadband Gr/InSe/MoTe2 heterostructure photodetectors with ultra-fast response and low dark current, Laser & Photonics Reviews 19(4) (2025) 2400480.
[26] L. Zhang, H. Huang, B. Zhang, M. Gu, D. Zhao, X. Zhao, L. Li, J. Zhou, K. Wu, Y. Cheng, Structure and properties of violet phosphorus and its phosphorene exfoliation, Angewandte Chemie 132(3) (2020) 1090-1096.
[27] S.S. Chee, D. Seo, H. Kim, H. Jang, S. Lee, S.P. Moon, K.H. Lee, S.W. Kim, H. Choi, M.H. Ham, Lowering the Schottky barrier height by graphene/Ag electrodes for high-mobility MoS2 field-effect transistors, Advanced Materials 31(2) (2019) 1804422.
[28] Y. Yang, S.C. Liu, X. Wang, Z. Li, Y. Zhang, G. Zhang, D.J. Xue, J.S. Hu, Polarization-sensitive ultraviolet photodetection of anisotropic 2D GeS2, Advanced Functional Materials 29(16) (2019) 1900411.
[29] D. Xie, G. Gao, B. Tian, Z. Shu, H. Duan, W.W. Zhao, J. He, J. Jiang, Porous metal–organic framework/ReS2 heterojunction phototransistor for polarization - sensitive visual adaptation emulation, Advanced Materials 35(26) (2023) 2212118.
[30] J. Tao, W. Shen, S. Wu, L. Liu, Z. Feng, C. Wang, C. Hu, P. Yao, H. Zhang, W. Pang, Mechanical and electrical anisotropy of few-layer black phosphorus, ACS nano 9(11) (2015) 11362-11370.

[31] E. Liu, Y. Fu, Y. Wang, Y. Feng, H. Liu, X. Wan, W. Zhou, B. Wang, L. Shao, C.-H. Ho, Integrated digital inverters based on two-dimensional anisotropic ReS2 field-effect transistors, Nature communications 6(1) (2015) 1-7.
[32] W. Ahmad, A. El Moutaouakil, W. Lei, Z.-M. Wang, 2D PdSe2: Pioneering innovations in polarized photodetection, Journal of Electronic Science and Technology (2025) 100305.
[33] X. Zhou, X. Hu, B. Jin, J. Yu, K. Liu, H. Li, T. Zhai, Highly anisotropic GeSe nanosheets for phototransistors with ultrahigh photoresponsivity, Advanced Science 5(8) (2018) 1800478.
[34] L. Pi, C. Hu, W. Shen, L. Li, P. Luo, X. Hu, P. Chen, D. Li, Z. Li, X. Zhou, Highly in-plane anisotropic 2D PdSe2 for polarized photodetection with orientation selectivity, Advanced Functional Materials 31(3) (2021) 2006774.
[35] G. Li, S. Yin, C. Tan, L. Chen, M. Yu, L. Li, F. Yan, Fast photothermoelectric response in CVD-grown PdSe2 photodetectors with in-plane anisotropy, Advanced Functional Materials 31(40) (2021) 2104787.
[36] C. Yan, K. Yang, H. Zhang, Y. Chen, H. Liu, High performance self-powered photodetector based on van der Waals heterojunction, Nanotechnology 35(3) (2023) 035203.
[37] W. Su, S. Zhang, C. Liu, Q. Tian, X. Liu, K. Li, Y. Lv, L. Liao, X. Zou, Interlayer transition induced infrared response in ReS2/2D perovskite van der Waals heterostructure photodetector, Nano Letters 22(24) (2022) 10192-10199.
[38] Y. Tang, H. Hao, Y. Kang, Q. Liu, Y. Sui, K. Wei, X.a. Cheng, T. Jiang, Distinctive interfacial charge behavior and versatile photoresponse performance in isotropic/anisotropic WS2/ReS2 heterojunctions, ACS Applied Materials & Interfaces 12(47) (2020) 53475-53483.
[39] K. Li, C. Du, H. Gao, T. Yin, L. Zheng, J. Leng, W. Wang, Ultrafast and polarization-sensitive ReS2/ReSe2 heterostructure photodetectors with ambipolar photoresponse, ACS Applied Materials & Interfaces 14(29) (2022) 33589-33597.
[40] C. Zhang, B. Zheng, G. Wu, X. Liu, J. Wu, C. Yao, Y. Wang, Z. Tang, Y. Chen, L. Fang, Controlled growth of vertically stacked In2Se3/WSe2 heterostructures for ultrahigh responsivity photodetector, Nano Research 17(3) (2024) 1856-1863.
[41] J. Yan, X. Yang, X. Liu, C. Du, F. Qin, M. Yang, Z. Zheng, J. Li, Van der Waals heterostructures with built-in Mie resonances for polarization-sensitive photodetection, Advanced Science 10(9) (2023) 2207022.
[42] A. Varghese, D. Saha, K. Thakar, V. Jindal, S. Ghosh, N.V. Medhekar, S. Ghosh, S. Lodha, Near-direct bandgap WSe2/ReS2 type-II pn heterojunction for enhanced ultrafast photodetection and high-performance photovoltaics, Nano letters 20(3) (2020) 1707-1717.
[43] J. Wang, C. Liu, L. Zhang, J. Chen, J. Chen, F. Yu, Z. Zhao, W. Tang, X. Li, S. Zhang, Selective Enhancement of Photoresponse with Ferroelectric-Controlled BP/In2Se3 vdW Heterojunction, Advanced Science 10(11) (2023) 2205813.
[44] W. Cai, J. Wang, Y. He, S. Liu, Q. Xiong, Z. Liu, Q. Zhang, Strain-modulated photoelectric responses from a flexible α-In2Se3/3R MoS2 heterojunction, Nano-Micro Letters 13(1) (2021) 74.
[45] W. Wu, Z. Liu, Z. Qiu, Z. Wu, Z. Li, X. Yang, L. Han, C. Li, N. Huo, X. Wang, An ultrasensitive ReSe2/WSe2 heterojunction photodetector enabled by gate modulation and its development in polarization state identification, Advanced Optical Materials 12(2) (2024) 2301410.
[46] J. Zou, Y. Ke, X. Zhou, Y. Huang, W. Du, L. Lin, S. Wei, L. Luo, H. Liu, C. Li, Broadband Visible–Near Infrared Two - Dimensional WSe2/In2Se3 Photodetector for Underwater Optical Communications, Advanced Optical Materials 10(12) (2022) 2200143.

[47] H. Li, K. Zhang, X. Li, B. Liu, L. Li, Z. Mei, T. Chen, Q. Liu, W. Yu, J. Yuan, Two-dimensional (2D) α-In2Se3/Ta2NiSe5 heterojunction photodetector with high sensitivity and fast response in a wide spectral range, Materials & Design 227 (2023) 111799.
[48] W. Ahmad, M.U. Rehman, U. Younis, A. Abbas, J. Kazmi, O.H.A. Suwaidi, Y.A. Samad, W. Lei, A.I. Channa, Q. Liang, Interlayer charge transition and broadband polarization photodetection and imaging based on In2Se3/ReS2 van der Waals heterostructure, Laser & Photonics Reviews 19(1) (2025) 2400819.
[49] Y. Wang, Z. Lai, S. Tang, J. Wang, Q. Zhou, S. Li, W. Wang, H. Zhao, Y. Yu, L. Gao, ReS2/MoSe2 Van der Waals Heterostructure Photodetectors for Polarization Imaging and Polarization-Encoded Optical Communication, Small 2503599.
[50] M.A. Stepanov, A.A. Guskov, R.R. Galiev, D.A. Abdullaev, E.S. Shahurin, S.D. Lavrov, E.D. Mishina, MoS2-based polarization-sensitive photodetectors with asymmetric plasmonic structures and decreased detection time, Optical Materials 152 (2024) 115452.